Optics Letters

Ultra-sensitive UV solar-blind optical wireless communications with an SiPM

Feng Liu,[1,*] James Farmer,[1] Andy Schreier,[1,2] Grahame Faulkner,[1] Hyunchae Chun,[1,3] William Matthews,[1] Zhaoming Wang,[1] and Dominic O'Brien[1,4]

[1]Department of Engineering Science, University of Oxford, Parks Road, Oxford OX1 3PJ, UK
[2]Fraunhofer Institute for Telecommunications Heinrich Hertz Institute, Berlin, Germany
[3]Department of Information and Telecommunication Engineering, Incheon National University, Incheon, Republic of Korea
[4]dominic.obrien@eng.ox.ac.uk
*feng.liu@eng.ox.ac.uk

Received 15 August 2023; revised 13 September 2023; accepted 22 September 2023; posted 22 September 2023; published 10 October 2023

In this Letter, an SiPM with a dedicated cooling system suitable for receiving ultra-low-power solar-blind wavelengths is reported. This is designed to decrease the temperature of the detector from 21°C to –10°C, and the corresponding dark count rate (DCR) is reduced by approximately 10 dB. A 275 nm optical wireless communication (OWC) system is established using on–off-keying (OOK) modulation. Transmission rates ranging from 100 kbit/s to 2 Mbit/s are demonstrated with this cooled SiPM. The received power is as low as 30 pW (corresponding to 41.5 photons per bit) at a data rate of 1 Mbit/s and a bit error rate of 2.4×10^{-3}.

https://doi.org/10.1364/OL.503235

Wireless communication is a critical technology for connecting users to an infrastructure, and current wireless communication services are mainly based on radio frequency (RF) approaches [1]. However, the RF spectrum is limited, so exploring higher-frequency spectrum resources is valuable to further improve the wireless communication service. Optical wireless communication (OWC) offers high bandwidth, low latency, robustness to electromagnetic interference, and no regulatory requirements [2]. A state-of-art research has demonstrated over 100 Tbit/s OWC [3]. Thus, OWC has great potential to provide wireless communication services in emerging technologies requiring ultra-high data rates, such as a virtual reality (VR) and an augmented reality (AR) [4]. In OWC, silicon photomultipliers (SiPMs) are one type of photon detectors. SiPMs are not originally designed for communications, but they offer high sensitivity. Recent research has shown over 1 Gbit/s links using SiPMs [5,6]. There are typically three bands used for OWC: the infrared (IR) band (750 nm–1 mm), the visible band (390–750 nm), and the ultraviolet (UV) band (10–390 nm). Within the UV band, there is a solar-blind spectral band covering 200 to 280 nm, whose corresponding radiation reaching the ground is extremely low, less than 5×10^{-23} W/(m^2·nm) [7]. Thus, wavelengths in this solar-blind spectrum offer a potential solution for OWC, as there is no sunlight interference. Corresponding links providing over 1 Gbit/s have been demonstrated [8,9].

However, compared to visible and IR light, the acceptable irradiance of the UV light for safety is lower. According to skin and eye-safety standards, the irradiance of light between 200 and 400 nm should be no more than 1 mW/m^2 [10]. Thus, to build OWC in the UV solar-blind region, improving receiver sensitivity to allow low transmission power is a key step. Recent UV solar-blind communication link demonstrations use received power levels of microwatts, corresponding to ~10^4 photons per bit [11,12]. For these demonstrations, the corresponding beam irradiance (considering the detected power divided by the receiver collection area) is estimated to be more than 10 mW/m^2, exceeding the eye-safety irradiance levels. Improving receiver sensitivity is therefore a key area of interest. In this Letter, an SiPM receiver which operates at ~40 photons per bit is reported, showing the promise of these devices for solar-blind links. To the best of our knowledge, this is the most sensitive UV solar-blind communication-oriented receiver reported thus so far.

The rest of this Letter is organized as follows. The operation of the SiPM is described, and the cooling arrangements and resulting improvement in performance detailed. A communication link that uses the SiPM is then reported, showing improved sensitivity with temperature. Conclusions and future work are then detailed.

The receiver detects signals by counting pulses generated by the SiPM. The SiPM is an array of single-photon avalanche diodes (SPAD). For each SPAD, a detected photon or a dark count causes avalanche multiplication and in turn generates a pulse, corresponding to a photon pulse or a dark pulse. In this Letter, the dead time of each SPAD within the SiPM is short (~20 ns), and the numbers of detected photons and dark count per bit are very low; the distribution of pulses follows a Poisson distribution [13]. The SPADs work in parallel and the pulses from different SPADs can be superimposed. Whether "1" or "0" is detected depends on whether there is any pulse within the detection window. If there is one pulse or more, the received bit is determined as "1." Based on the Poisson distribution of

detected photons and dark counts, there are two categories of noises causing errors. (1) Dark noise: the dark pulses fall in the detection window, so the transmitted "0" is detected as "1." (2) No-photon Poisson noise: no photons are detected because of Poisson distribution, so the transmitted "1" is detected as "0."

The BER considering temperature change is derived as follows. The probability of detecting dark pulses is

$$P_d = 1 - \frac{(R_d \cdot t_d)^0}{0!} e^{-R_d \cdot t_d} = 1 - e^{-R_d \cdot t_d}, \tag{1}$$

where R_d and t_d are the dark count rate (DCR) and the time duration of the detection window, respectively. The DCR changes with temperature [14]:

$$R_\mathrm{d} = R_0 \cdot 10^{\frac{T-T_0}{\alpha}}, \tag{2}$$

where T_0 and R_0 are room temperature and DCR under room temperature, respectively. α is the temperature factor of DCR, which is 30°C for silicon-based SiPMs [14]. Equation (2) assumes a constant overvoltage (bias voltage–breakdown voltage) and therefore a constant photon detection efficiency (PDE) and a constant gain. The relationship between the breakdown voltage and temperature is [14]

$$V_\mathrm{b} = V_{\mathrm{b}0} - \beta \cdot (T_0 - T), \tag{3}$$

where $V_{\mathrm{b}0}$ is the breakdown voltage under room temperature. β is the temperature factor of breakdown voltage. The error probability due to bits "1" without detected photons is [15]

$$P_\mathrm{n} = \frac{1}{2} \cdot \frac{\mu^0}{0!} e^{-\mu} = \frac{1}{2} e^{-\mu}, \tag{4}$$

where μ is the average number of detected photons for a bit "1," which can be obtained from

$$\mu = 2 \cdot \mathrm{PDE} \cdot P/(h \cdot c/\lambda)/R, \tag{5}$$

where PDE and P are the photon detection efficiency and the received power of the SiPM, respectively. h is Planck's constant and c is the speed of light. λ is the operating wavelength and R is the data rate. Thus, the total bit error rate BER is the combination of these two errors:

$$\mathrm{BER} = \frac{1}{2} P_\mathrm{d} + P_\mathrm{n} - P_\mathrm{d} \cdot P_\mathrm{n}. \tag{6}$$

The factor $1/2$ originates from the 50% probability of dark pulses occurring in bits "1," which will not cause an error. $P_\mathrm{d} \cdot P_\mathrm{n}$ is the probability that bits "1" are correctly detected due to dark pulse instead of detected photons.

The experimental schematic is shown in Fig. 1. The transmitter is a UV LED operating at 275 nm (Thorlabs LED275J) driven by an arbitrary waveform generator (AWG, AGILENT 81150A) transmitting OOK optical signals. In the receiver, the SiPM (a 3×3 mm HAMAMATSU UV-sensitive SiPM, S13360-2226) is installed on a cooling setup, which can reduce the temperature of the SiPM to approximately −10°C. A source meter (KEITHLEY 2636B) provides bias voltage to the SiPM and measures the current flowing through the device. The SiPM's photocurrent is amplified using an ADA4817 trans-impedance amplifier (TIA). This amplified signal is passed to an oscilloscope (AGILENT MSO6104A) for data capture. The AWG, source meter, and oscilloscope are remotely controlled by a PC, and the captured data is post-processed offline. The distance between the

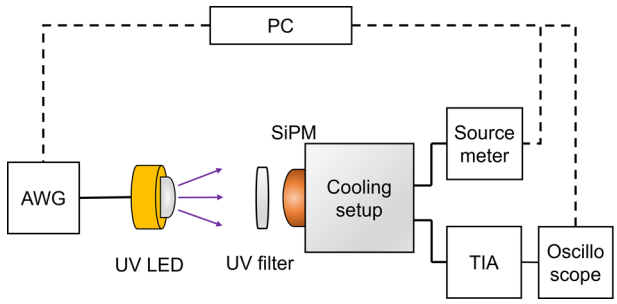

Fig. 1. Experiment schematic for 275 nm OWC link.

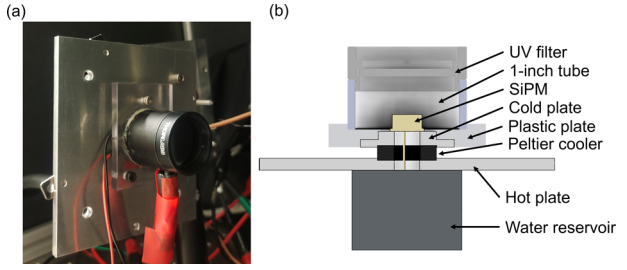

Fig. 2. Cooling setup design. (a) Photograph. (b) Sectional view.

UV LED and the SiPM is 10 cm. A UV bandpass filter (Thorlabs FGUV5M) is used in front of the SiPM to make a sealed space.

The cooling setup is the key to reducing the dark current, and in turn, decreasing the BER. A photograph and a sectional view of the cooling setup are shown in Figs. 2(a) and 2(b), respectively. A Peltier element cools the SiPM through an aluminum (Al) plate, which is held in place by a plastic plate. A 1 in. tube with a UV filter on top creates a sealed space to avoid condensation. The hot side of the Peltier consists of a large Al plate and a water reservoir fed by a CPU cooler.

The capability of the cooling setup is characterized by measuring the dark current as a function of temperature and bias voltage as shown in Fig. 3(a). The breakdown voltage of the detector decreases with decreasing temperatures by 54 mV/K. To keep a constant overvoltage, the bias voltage must be adjusted according to the temperature setting. Thus, at −10°C the bias voltage is set to 55.2 V, resulting in a measured dark current of 3.9 nA compared to 56.8 V and 42 nA at 21°C. Those measurement values correspond to a reduction in the dark current of about 10 dB within 30 K of cooling. This gradient agrees with previously reported values for SiPMs [14]. The gain of the SiPM can be obtained by measurement based on the principle shown in [16]

$$G = \frac{I_\mathrm{d}}{R_\mathrm{d} \cdot e_0}, \tag{7}$$

where I_d is the dark current and e_0 is the elementary charge. The gain of the SiPM is calculated as approximately 7×10^5.

The photocurrent of the SiPM is plotted as a function of irradiances from the UV LED in Fig. 3(b), considering SiPM temperature of 21°C and −10°C. As the plots for both temperature settings fit each other well, the gain and the PDE of the SiPM can be considered constant when accounting for breakdown voltage adjustments. The PDE can be obtained by measurement based on the principle shown in [16]

$$\mathrm{PDE} = \frac{(I_\mathrm{t} - I_\mathrm{d}) \cdot h \cdot c}{G \cdot e_0 \cdot E \cdot A \cdot \lambda}, \tag{8}$$

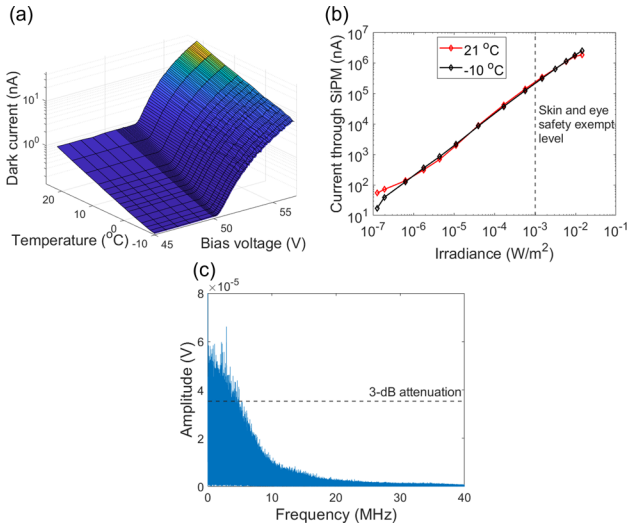

Fig. 3. Receiver characterization. (a) Dark current versus temperature and bias voltage. (b) Current through SiPM versus irradiance. (c) Frequency domain plot of dark pulses.

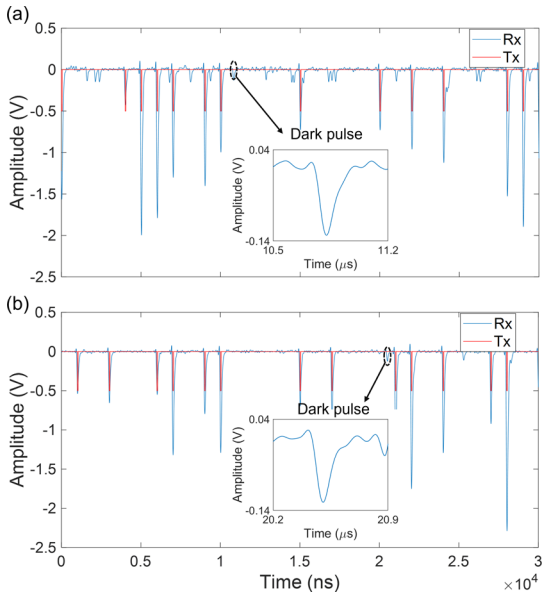

Fig. 4. Transmitted sequence and synchronized received pulses at (a) 21°C and (b) −10°C. (Note: The values of received pulses are negative, due to the nature of the TIA circuit to the input current from the SiPM.)

where I_t is the total current through SiPM, including photocurrent and dark current. E is the irradiance and A is the detection area of SiPM. The PDE is calculated as 15.38%.

The electrical bandwidth of the transmitter is measured as approximately 9 MHz, using a high bandwidth (>100 MHz) UV-APD as a reference detector and modulating the source using a swept frequency signal generator. The LED is biased to operate in its linear region using a current source (laser driver), and a bias T combines the modulation and bias. The receiver electrical bandwidth is determined by Fourier transforming the received dark current signal of the SiPM. This is shown in Fig. 3(c), and the 3 dB bandwidth is approximately 5 MHz.

During the link demonstration, the PRBS sequences are modulated and transmitted as OOK signals. The OOK signals are detected and synchronized by correlating the transmitted PRBS sequences and received pulses. The bit decision is achieved by comparing the values of received pulses within the detection window to the decision threshold. The decision threshold is set as −125 mV, corresponding to approximately 90% of the single pulse's peak value to ensure the counts from pulses with irregular shapes, without losing generality. Specifically, in the transmitter, the data rate ranges from 100 kbit/s to 2 Mbit/s, and the corresponding duty cycles are listed in Table 1. The detection window is fixed at 50 ns, which leads to a variation in the duty cycle as the bit rate changes. The value of the detection window is chosen as a trade-off between collecting sufficient power (leading to a longer window) and minimizing the dark counts recorded (favoring a shorter window). In the receiver, both 21°C and −10°C conditions are considered, and the corresponding bias voltages are 56.8 and 55.2 V, respectively. The overvoltage is constant, so the PDE and gain are fixed at 15.38% and 7×10^5, respectively. In the communication link, with the fixed data rate of 1 Mbit/s, the BER is measured with the received power ranging from 10 to 40 nW. Then, the links

Table 1. Duty Cycle for Different Data Rates

Data Rate (Mbit/s)	0.1	0.2	0.5	1	2
Duty Cycle (%)	0.5	1	2.5	5	10

at different data rates, from 100 kbit/s to 2 Mbit/s, are tested with the fixed received power per bit (41.5 photons per bit). The standard quantum limit for OOK is 3.5 detected photons per bit at a BER of 1×10^3 based on Poisson distribution [15]. In this Letter, for 41.5 incident photons per bit, 6.38 detected pulses would be expected ($41.5 \times 15.38\ \% = 6.38$), which is close to (approximately twice) the quantum limit.

Figure 4 shows the communication link data with both transmitted sequences and synchronized received pulses. The data rate is 1 Mbit/s, and the received power is 30 pW (corresponding to 41.5 photons per bit). This experiment is conducted at 21°C and −10°C, and the data is displayed over 30 μs. In the transmitted sequence (red line), the value −0.5 V represents the transmitted bit "1." In the received pulses (blue line), the amplitude of each "1" bit has different amplitudes due to the varying number of detected photons in each bit. The figure shows that the transmitted sequence and the received pulses match very well. The zoomed single dark pulses in Figs. 4(a) and 4(b) are nearly identical, including the shape and amplitude, because of the unchanged overvoltage. Moreover, it can be observed that the number of dark pulses is reduced from 21°C to −10°C.

The BER versus the received power and temperature are plotted in Fig. 5 with the data rate of 1 Mbit/s. Moreover, the forward correction threshold is indicated. Each BER point is obtained by transmitting 50×2^{10} bits. The results show that the BER at −10°C is always lower than the BER at 21°C due to the reduction of DCR. For the received powers over 23 pW at −10°C, the BER is below the forward correction threshold. The two BER curves drop to a minimum value (2.4×10^{-3} with 30 pW at −10°C) because the no-photon Poisson noise dominates and decreases as the temperature reduces. The two BERs slightly increase for the received powers exceeding 30 pW, and this is caused by afterpulses. Afterpulses are delayed pulses following output signal pulses, which are generated with a specific probability when a threshold current through SiPMs is exceeded, as

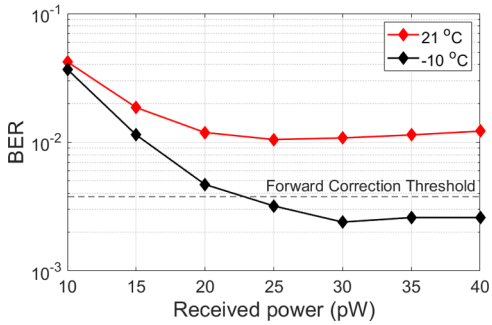

Fig. 5. BER versus received power and temperature.

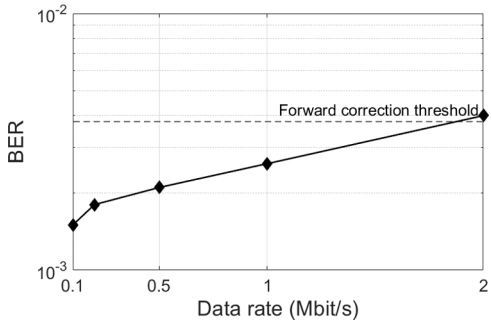

Fig. 6. BER versus data rate at −10°C.

a result of the high received optical power. Due to the bandwidth limitation of the receiver, a portion of the time-domain waveform of the afterpulses falls into the detection window of the next bit, causing the transmitted "0" to be detected as "1." Increasing the received power increases the proportion of signal pulses exceeding the afterpulses threshold and, in turn, increases the number of afterpulses.

The BER versus data rate is shown in Fig. 6. It can be seen that the BER increases with increasing data rate resulting in BER at 2 Mbit/s exceeding the forward correction threshold, due to higher data rates, increasing the probability of afterpulses. Additionally, inter-symbol interference (ISI) occurs at higher data rates because the response of the receiver is longer than the bit window [17].

In conclusion, this Letter demonstrates an ultra-sensitive UV solar-blind OWC scheme at 275 nm. The receiver (a cooled SiPM with the temperature of −10°C) operates at ∼40 photons per bit. Compared with more typical levels of 10^4 photons per bit found in recent demonstrations [11,12], the sensitivity is improved by approximately 240 times. The communication link of 1 Mbit/s is demonstrated with a received power of 30 pW (corresponding to 41.5 photons per bit) and a BER of 2.4×10^{-3}.

Future work will further increase the data rate by improving receiver bandwidth and applying equalization to deal with ISI.

Disclosures. The authors declare no conflicts of interest.

Data availability. Data underlying the results presented in this paper are not publicly available at this time but may be obtained from the authors upon reasonable request.

REFERENCES

1. S. Elmeadawy and R. M. Shubair, in *2019 International Conference on Electrical and Computing Technologies and Applications (ICECTA)* (2019), pp. 1–5.
2. Z. Ghassemlooy, S. Arnon, M. Uysal, Z. Xu, and J. Cheng, IEEE J. Select. Areas Commun. **33**, 1738 (2015).
3. H. Huang, G. Xie, Y. Yan, N. Ahmed, Y. Ren, Y. Yue, D. Rogawski, M. J. Willner, B. I. Erkmen, K. M. Birnbaum, S. J. Dolinar, M. P. J. Lavery, M. J. Padgett, M. Tur, and A. E. Willner, Opt. Lett. **39**, 197 (2014).
4. O. Bouchet, M. Lanoiselée, D. O'Brien, R. Singh, M. Ghoraishi, R. Perez, V. Guerra, S. Topsu, and J. Garcia-Marquez, *Terabit Per Second Optical Wireless Links for Virtual Reality Technology* (SPIE, 2018).
5. W. Matthews, Z. Ahmed, W. Ali, and S. Collins, IEEE Photonics Technol. Lett. **33**, 487 (2021).
6. S. Huang, C. Chen, R. Bian, H. Haas, and M. Safari, Opt. Lett. **47**, 2294 (2022).
7. National Renewable Energy Laboratory, "Reference air mass 1.5 spectra," https://www.nrel.gov/grid/solar-resource/spectra-am1.5.html.
8. O. Alkhazragi, F. Hu, P. Zou, Y. Ha, Y. Mao, T. K. Ng, N. Chi, and B. S. Ooi, in *Optical Fiber Communication Conference (OFC)* (Optica Publishing Group, 2020), paper M3I.5.
9. K. Kojima, Y. Yoshida, M. Shiraiwa, Y. Awaji, A. Kanno, N. Yamamoto, and S. Chichibu, in *2018 European Conference on Optical Communication (ECOC)* (2018), p. 1.
10. British Standards Institution, "Photobiological safety of lamps and lamp systems," BS EN 62471:2008 (2008).
11. S. Zhu, P. Qiu, Z. Qian, X. Shan, Z. Wang, K. Jiang, X. Sun, X. Cui, G. Zhang, D. Li, and P. Tian, Opt. Lett. **46**, 2147 (2021).
12. D. M. Maclure, J. J. D. McKendry, M. S. Islim, E. Xie, C. Chen, X. Sun, X. Liang, X. Huang, H. Abumarshoud, J. Herrnsdorf, E. Gu, H. Haas, and M. D. Dawson, Photonics Res. **10**, 516 (2022).
13. E. Sarbazi, M. Safari, and H. Haas, IEEE Trans. Commun. **68**, 5689 (2020).
14. A. N. Otte, D. Garcia, T. Nguyen, and D. Purushotham, Nucl. Instrum. Methods Phys. Res., Sect. A **846**, 106 (2017).
15. D. Hall, Y. H. Liu, L. Yan, Y. Yu, and Y. H. Lo, IEEE Trans. Electron Devices **64**, 4812 (2017).
16. G. Bonanno, P. Finocchiaro, A. Pappalardo, S. Billotta, L. Cosentino, M. Belluso, S. Di Mauro, and G. Occhipinti, Nucl. Instrum. Methods Phys. Res., Sect. A **610**, 93 (2009).
17. W. Matthews, W. Ali, Z. Ahmed, G. Faulkner, and S. Collins, IEEE Photonics Technol. Lett. **33**, 449 (2021).